Journal of Industrial and Engineering Chemistry 90 (2020) 358–370

Contents lists available at ScienceDirect

Journal of Industrial and Engineering Chemistry

journal homepage: www.elsevier.com/locate/jiec

Highly efficient photocatalytic oxidative desulfurization of dibenzothiophene with sunlight irradiation using green catalyst of Ag@AgBr/Al-SBA-15 derived from natural halloysite

Xuan Nui Pham[a,*], Manh B. Nguyen[b], Ha Son Ngo[a], Huan V. Doan[a,c,*]

[a] Department of Chemical Engineering, Hanoi University of Mining and Geology, 18 Vien Street, Bac Tu Liem District, Hanoi, Viet Nam
[b] Institute of Research and Development, Duy Tan University, Da Nang 550000, Viet Nam
[c] Department of Mechanical Engineering, University of Bristol, Bristol BS8 1TH, UK

ARTICLE INFO

Article history:
Received 5 May 2020
Received in revised form 15 July 2020
Accepted 18 July 2020
Available online 29 July 2020

Keywords:
Ag@AgBr
Photocatalytic degradation
DBT
Sunlight
Photocatalyst

ABSTRACT

In recent decades, highly efficient deep desulfurization processes have become very necessary to decrease environmental pollution due to sulfur emissions from fuels. Herein, an enhanced photocatalytic desulfurization of a model fuel was investigated under sunlight irradiation using H_2O_2 as the oxidant and Ag@AgBr loaded mesoporous silica Al-SBA-15 as a catalyst. In this study, the photocatalyst (Ag@AgBr/Al-SBA-15) was synthesized via a chemical deposition using halloysite clay as the silica–aluminum source and characterized by X-ray diffraction, N_2 adsorption, scanning electron microscopy, transmission electron microscopy, and UV–Vis diffuse reflectance spectroscopy (UV–Vis DRS). The UV–Vis DRS results revealed that the light absorption expanded to the visible region ($\lambda > 400$ nm) for the various Ag@AgBr nanoparticles doped in the mesoporous Al-SBA-15 material. The 30% Ag@AgBr/Al-SBA-15 sample with a 30% Ag@AgBr doping exhibited enhanced photocatalytic activity and showed high stability even after four successive cycles. The results demonstrated that initial dibenzothiophene concentrations (500 ppm) reached 98.66% removal with 50 mg of the catalyst dosage, 1.0 mL of H_2O_2, for 360 min of sunlight irradiation at 70 °C.

Introduction

Environmental pollution due to increasing harmful emissions is a global concern. One of the causes of air pollution is sulfur dioxide gas, which is formed from organic compounds containing sulfur in transportation fuels [1]. Traditional technology used to remove sulfur from liquid fuels is hydrodesulfurization (HDS). However, existing HDS technology requires a high temperature and high pressure and is less effective in removing organic sulfur compounds, such as thiophene (TH), benzothiophene (BT), dibenzothiophene (DBT), and alkyl substitute DBT, because of the steric hindrance effect [2]. Hence, researchers have recently concentrated their efforts on lowering the operating costs, and photocatalytic-oxidative desulfurization is one of the most promising alternative approaches.

For the past few decades, TiO_2 has been considered one of the most applicable and promising photocatalysts in "green chemistry". However, pure TiO_2 can only be excited by UV radiation, which accounts for 5% of the solar energy because of its high bandgap of approximately 3.0–3.2 eV [3–6]. Therefore, a photocatalyst that can be efficiently active and stable in the visible region is required. Theoretically, photocatalytic efficiency can be improved by the plasmonic surface resonance effect, which is created by the addition of a noble metal such as Au or Ag. Recently, 3D-MoS_2 sponge [7], metallic active site on MoO_2(1 0 0) surface [8], singlet oxygen triggered by superoxide radicals in molybdenum [9] have been proposed as excellent cocatalysts in advanced oxidation processes for pollutant control. Au- and Ag-based photocatalysts, such as Au/SBA-15 [10], Ag/SBA-15 [11], Ag@C_3N_4 [12], Ag/ZnO [13], C/TiO_2@CM-41 [14], and ZnO-based visible-light-driven photocatalysts have been reviewed for the degradation of different pollutants [15,16]. Ag@AgBr, g-C_3N_4-based nanocomposites are also promising visible-light-driven photocatalysts for environmental pollution remediation, production and storage of energy and gas sensors [17,18], and production of value-added chemicals [19,20].

* Corresponding authors at: Department of Chemical Engineering, Hanoi University of Mining and Geology, 18 Vien Street, Bac Tu Liem District, Hanoi, Viet Nam.
E-mail addresses: phamxuannui@humg.edu.vn, phamxuannui@gmail.com (X.N. Pham), huan.doan@bristol.ac.uk (H.V. Doan).

https://doi.org/10.1016/j.jiec.2020.07.037
1226-086X/

Among them, the Ag–AgBr photocatalyst is known as a narrow-gap semiconductor for building a heterostructure system, which has been proposed as a highly efficient photocatalytic material under visible light irradiation [21,22]. This efficiency is due to the plasmonic surface interaction of silver nanoparticles that can effectively increase the interparticle electron transfer and inhibit the recombination of the photogenerated electrons and holes. Furthermore, it can create a synergistic effect with the photosensitive characteristic of AgBr [23,24].

However, the photocatalytic activity of Ag–AgBr is limited because of the large particle size, which is approximately several micrometers. This can lead to a relatively small specific surface as well as a fast recombination of charged particles. Therefore, to utilize solar energy, Ag–AgBr should be distributed on supports that have a high specific surface area and are stable under reaction conditions. For example, Ag–AgBr was dispersed on activated carbon as a photocatalyst for the adsorption and degradation of Rhodamine B under visible light irradiation [25]. Entezari et al. [26] developed a new method by using ultrasonography for the synthesis of Ag/AgBr/graphene oxide with high adsorption-photocatalytic activity in the degradation of methyl orange. Dong et al. [27] synthesized Ag@AgBr/carbon nanotube nanocomposites by using the deposition–precipitation method for the photocatalytic reduction of CO_2 to chemical fuels. Hu et al. [28] prepared Ag@AgBr/SBA-15 using an impregnation decomposition process for the visible light photocatalytic degradation of the dye Rhodamine B in aqueous solutions.

Mesoporous silica SBA-15 is known for its high specific surface area, large pore volume, and narrow pore size distribution as well as high thermal and mechanical stability [29–31], which is favorable as a support for the dispersion of the active component. Researchers have synthesized mesoporous materials by using various silica sources, such as tetraethylorthosilicate (TEOS) or tetramethylorthosilicate (TMOS). However, the synthesized materials are an expensive and toxic silica source. Recently, mesoporous silica was synthesized with kanemite ($NaHSi_2O_5 3{\cdot}H_2O$) [32], metakaoline [33], coal fly ash [34], and bentonite [35]. In our previous research [22,36], we synthesized mesoporous silica Al-MCM-41 from natural bentonite with a BET surface area of 633 m^2/g, pore volume of 0.94 cm^3/g, and pore size of 8.64 nm, respectively. Halloysite was recently used as a silica and aluminum source to synthesize a mesoporous SBA-15 material. Yan et al. [37] made an ordered mesoporous aluminosilicate molecular sieve from natural halloysite with a BET surface area of 524.6 m^2/g and a pore volume of 0.87 cm^3/g by using a hydrothermal treatment.

The present work aimed to (i) synthesize the Al-SBA-15 from halloysite clay as aluminum–silica sources; (ii) synthesize nanocomposite Ag@AgBr/Al-SBA-15 with varying Ag@AgBr by chemical vapor deposition as the photocatalyst for the oxidative desulfurization of DBT; (iii) investigate the effects of the Ag@AgBr dispersion in the nanocomposite, reaction temperature, and amount of the H_2O_2 agent on the DBT degradation; and (iv) study the kinetics on the photocatalytic oxidative desulfurization of DBT by using Ag@AgBr/Al-SBA-15 and the regeneration and reusability of the Ag@AgBr/Al-SBA-15 photocatalyst.

Experimental

Materials

The raw halloysite, a special type of natural kaolin, was purchased from Yenbai Province, Vietnam. The chemical composition of halloysite was 32.26% SiO_2, 13.67% Al_2O_3, 4.38% Fe_2O_3, 0.39% TiO_2, 2.75% CuO, 1.25% MgO, 22.70% Na_2O, and 22.60% loss on ignition (LOI) (wt.%). Silver nitrate ($AgNO_3$), cetyltrimethylammonium bromide (CTABr), poly(ethylene glycol)-block-poly(propylene glycol)-block-poly(ethylene glycol) (P_{123}), hydrochloric acid (HCl), sodium hydroxide (NaOH), and hydrogen peroxide (H_2O_2) were obtained from Sigma–Aldrich. Dibenzothiophene (DBT) and *n*-octane (C_8H_{18}) were purchased from Merck. All the materials were used as received without additional treatment. Deionized water (DI) was used in all the synthesis processes.

Synthesis of photocatalyst

Synthesis of Al-SBA-15 from halloysite clay

Firstly, 10 g of natural halloysite was calcined at 700 °C (5 °C/min) for 3 h and then cooled down naturally at room temperature. The powder was then stirred at 500 rpm with 100 mL of NaOH for 24 h at 80 °C. Next, the product was washed several times with

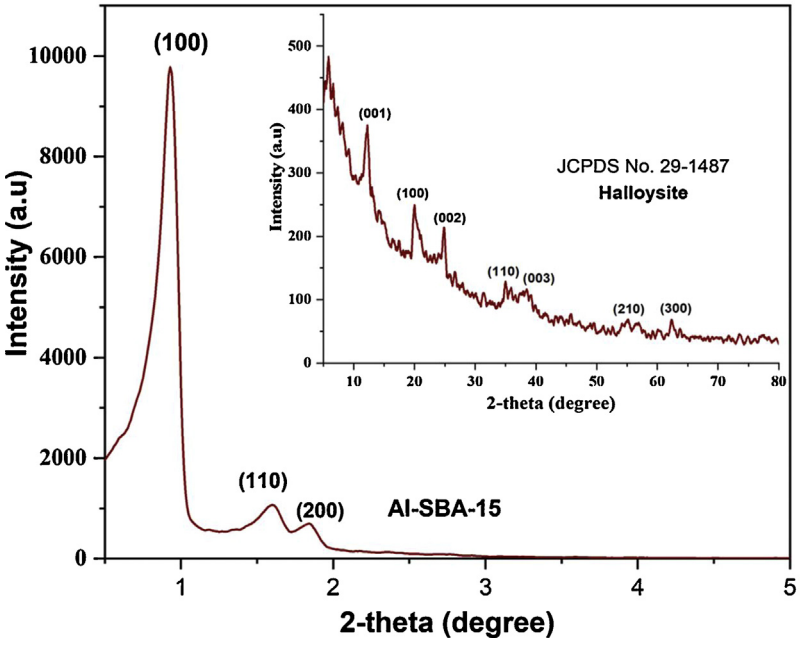

Fig. 1. Small-angle XRD of the synthesized Al-SBA-15 (inset: XRD pattern of natural halloysite).

distilled water to completely remove the residual NaOH and dried at 100 °C for 12 h. Finally, the silica precursor was obtained for the preparation of Al-SBA-15.

Secondly, 4 g of P123 was dissolved in 30 mL of distilled water with the addition of 120 mL of 2 M HCl, and the mixture was stirred at 500 rpm for 3 h at 40 °C. Then, 4 g of silica precursor was added and stirred continuously for 24 h. The solution was kept in an autoclave at 100 °C for 48 h. After aging, the sample was washed with distilled water and dried at 80 °C for 8 h. The obtained solid was calcined in air at 550 °C for 6 h with a heating rate of 5 °C/min.

Synthesis of Ag@AgBr/Al-SBA-15

x%Ag@AgBr/Al-SBA-15 samples with various Ag@AgBr weight percentage (*x* = 10%, 20%, 30%, 40%, 50%, and 60%) were synthesized using the chemical vapor deposition method, as in our previous research [22]. In brief, 0.9 g of Al-SBA-15, 0.5 g of CTABr, and 0.1574 g of $AgNO_3$ was sealed in glass wool and placed on each side of the quartz reactor. Then, the mixture was heated to 400 °C (5 °C/min) in the presence of N_2 (99.99%) with a flow rate of 60 mL/min for 3 h. In this process, the bromide ions from CTABr were used in an excess amount to precipitate Ag^+ from the $AgNO_3$ in the quartz reactor, which was adjusted by varying the $AgNO_3$ contents. The sample was washed with distilled water and dried at 80 °C for 8 h. The Ag@AgBr/Al-SBA-15 composites were achieved and used for further studies.

Characterization

The X-ray diffraction (XRD) patterns of the samples were obtained with D8 ADVANCE, Bruker, Germany, by using CuK_α radiation (λ = 1.540 Å). The small-angle data were collected in the 2θ angle range of 0.5–5° at a scan speed of 0.5° min^{-1}, and the wide-angle data were collected in the 2θ angle range of 10–80° at a scan speed of 5° min^{-1}. The specific BET surface area was determined with Automated Sorptometer BET 201-A, USA, by N_2 adsorption at 77.3 K. Scanning electron microscopy (SEM) images were obtained with an S-4800 microscope, Hitachi, Japan. Al-SBA-15 and Ag@AgBr/Al-SBA-15 nanocomposite powders were then examined using transmission electron microscopy (TEM, Leica IEO 906E). The UV–Vis diffuse reflectance spectra (DRS) were measured with a Shimadzu UV2550 spectrophotometer.

Photocatalytic performance of the samples

In the photocatalytic oxidative desulfurization experiments, direct sunlight was applied as the energy source. The photocatalytic activity of the as-synthesized Ag@AgBr/Al-SBA-15 nanocomposite was studied for the degradation of DBT in *n*-octane as the model fuel sample. In the test, 25 mL of DBT (500 ppm) and 25 mg of the catalyst were added to the Pyrex three-necked glass flask and magnetically stirred at 500 rpm. Before the photocatalytic activity began under sunlight irradiation, the mixture was placed in the dark for 60 min to attain the adsorption–desorption equilibrium between the DBT and the photocatalyst. The experiments were performed at different times and temperatures. Different amounts of the Ag@AgBr catalyst (10, 20, 30, 40, 50, and 60 wt.%) were investigated, and 30 wt.% was found to be the best choice for the active phase dosage of the photocatalyst. The degradation of DBT was determined based on the absorption at λ_{max} = 325 nm by using a UV–Vis spectrophotometer. The DBT concentrations at the equilibrium were taken as the initial concentration (C_0) for the DBT photocatalytic degradation.

Results and discussion

Characterization of samples

The mesoporous structures of Al-SBA-15 and natural halloysite were examined using the XRD patterns. Fig. 1 (inset) shows the peaks at 2θ values of 12.1°, 20.1°, 24.5°, 35.0°, 38.6°, 54.5°, and 62.5° corresponding to the diffraction of the (0 0 1), (1 0 0), (0 0 2), (1 1 0), (0 0 3), (2 1 0), and (3 0 0) planes of the halloysite with JCPDS Card No. 29-1487. The small-angle XRD patterns of the synthesized Al-SBA-15 sample showed the characteristics of three distinct diffraction peaks in the 2θ range of 0.5–2.0°, indexed as the (1 0 0), (1 1 0), and (2 0 0) planes of the two-dimensional (2D) hexagonal p6mm structure. The wide-angle XRD patterns showed only typical amorphous silica at 2θ of 23°, indicating that the support was an amorphous phase [38,39].

The phase structure and the crystallinity of the as-synthesized nanocomposite are given in Fig. 2. All the small-angle XRD patterns of 10–60%Ag@AgBr/Al-SBA-15 (Fig. 2A) showed the characteristic 2D hexagonal structure p6mm, and the Ag@AgBr/Al-SBA-15

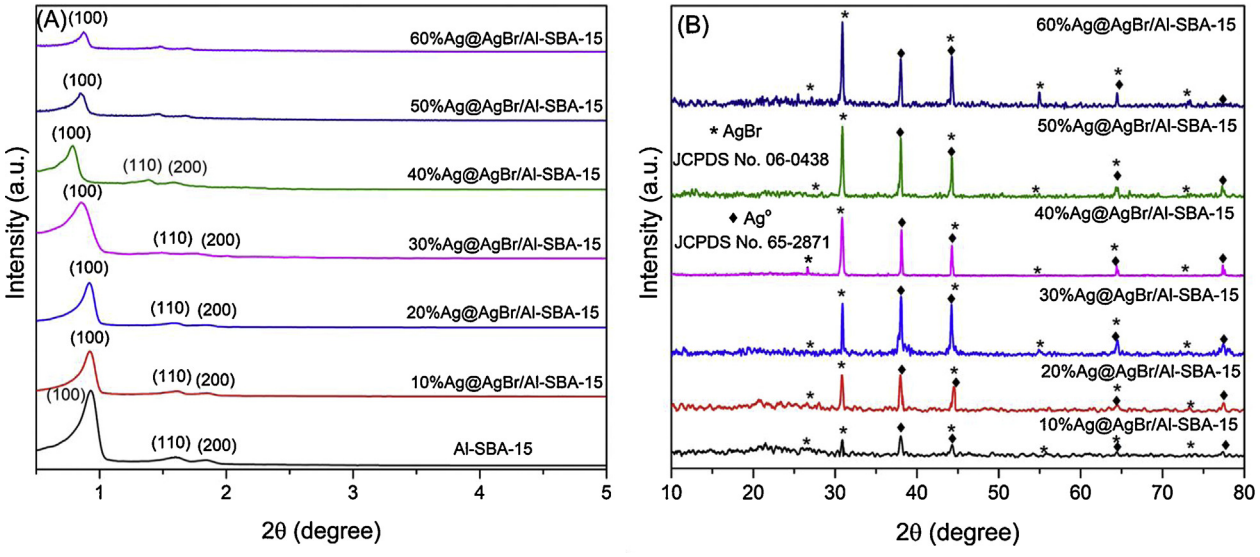

Fig. 2. (A) Small-angle and (B) wide-angle of XRD patterns of 10–60%Ag@AgBr/Al-SBA-15 samples.

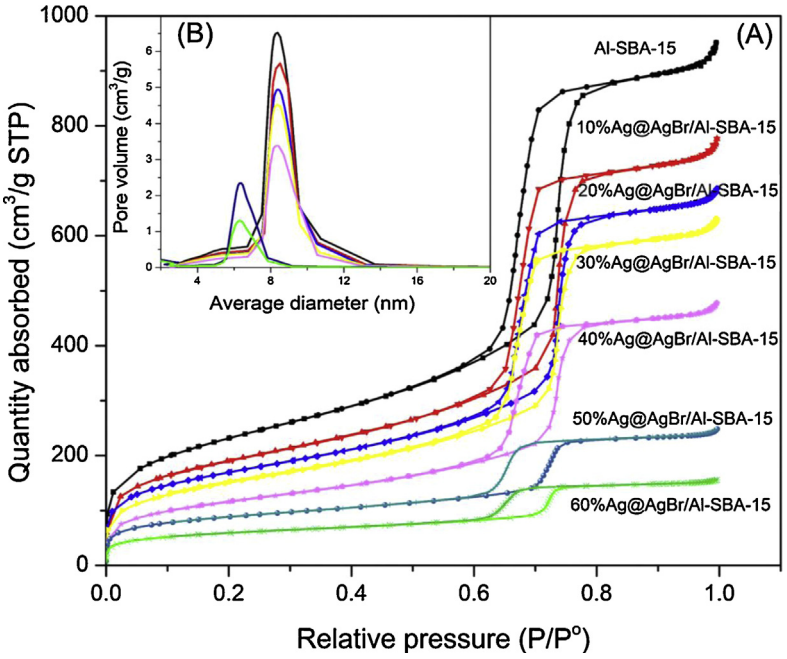

Fig. 3. (A) N_2 adsorption–desorption isotherms, and (B) pore size distribution of Al-SBA-15 and 10–60%Ag@AgBr/Al-SBA-15 samples.

maintained the structure of Al-SBA-15. However, the intensity of the diffraction peaks in Ag@AgBr/Al-SBA-15 was lower than that of Al-SBA-15, which might be attributed to the formation of Ag@AgBr inside the channels of Al-SBA-15 [40].

The wide-angle XRD patterns of the Ag@AgBr/Al-SBA-15 samples with different Ag@AgBr wt.% are shown in Fig. 2B. We observed that all the samples possessed both Ag and AgBr phases. The diffraction peaks at approximately 38.1°, 44.3°, 64.5°, and 77.5° (marked with "•") corresponded to the (1 1 1), (2 2 0), (4 0 0), and (3 1 1) crystal planes of Ag^0 (JCPDS No. 65-2871). The peaks at approximately 26.7°, 31.0°, 44.3°, 55.0°, 64.5°, and 73.4° (marked with "*") could be assigned to the (1 1 1), (2 0 0), (2 2 0), (2 2 2), (4 0 0), and (4 2 0) (JCPDS Card No. 06-0438) crystal planes of AgBr. This suggested that Ag^0 and AgBr co-existed in the Ag@AgBr/Al-SBA-15 nanocomposite.

The N_2 adsorption–desorption isotherm and JBH pore size distribution curves of the Al-SBA-15 and Ag@AgBr/Al-SBA-15 samples also exhibited type IV with H_1 hysteresis loops according to the IUPAC classification, as shown in Fig. 3. The N_2 physisorption data of the samples are shown in Table 1. The results showed a remarkable decrease in pore diameter in the case of 40–60% Ag@AgBr/Al-SBA-15. This could be illustrated by the insertion of the Ag@AgBr content into the mesoporous system of Al-SBA-15 that decreased the pore diameter. Meanwhile, no significant

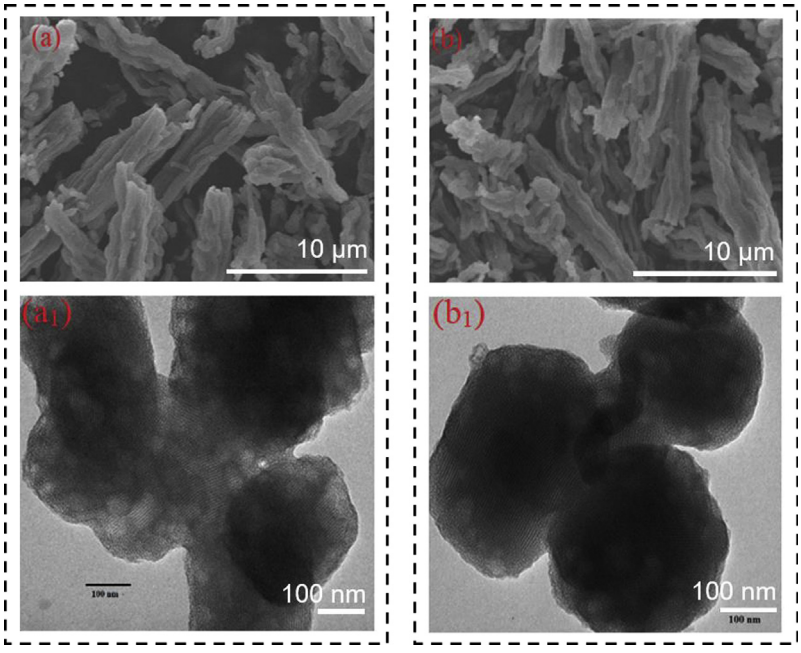

Fig. 4. SEM and TEM images of (a, a_1) Al-SBA-15 and (b, b_1) 30%Ag@AgBr/Al-SBA-15 samples.

Table 1
Textural properties of Al-SBA-15 and 10–60%Ag@AgBr/Al-SBA-15 samples.

Samples	BET specific surface area (m^2/g)	Pore volume (cm^3/g)	Average pore size (nm)
Al-SBA-15	819	1.50	8.15
10%Ag@AgBr/Al-SBA-15	672	1.21	8.14
20%Ag@AgBr/Al-SBA-15	594	1.10	8.13
30%Ag@AgBr/Al-SBA-16	530	1.01	8.07
40%Ag@AgBr/Al-SBA-17	412	0.75	8.04
50%Ag@AgBr/Al-SBA-18	302	0.40	6.50
60%Ag@AgBr/Al-SBA-19	202	0.22	6.20

difference in the N_2 adsorption–desorption curves between the samples of 10–30%Ag@AgBr/Al-SBA-15 and the Al-SBA-15 support were found.

The results shown in Table 1 revealed that the specific surface area of nanocomposite Ag@AgBr/Al-SBA-15 was smaller than that of Al-SBA-15. That is, the value decreased from 819 to 202 m^2/g depending on the amount of Ag@AgBr inserted. Moreover, the pore diameter and volume decreased along with the specific surface area. As described, the pore volume of the AgBr/Al-SBA-15 samples was lower than that of Al-SBA-15, and a sixfold decrease was recorded when the quantity of Ag@AgBr was increased from 10% to 60%. Meanwhile, only a slight change in the pore diameter was observed with the variation of the Ag@AgBr loading. This could be attributed to the uniform dispersion of Ag@AgBr onto Al-SBA-15. In addition, the formation of mesopores between the Ag particles might have kept the pore diameter unchanged in the 10–30% Ag@AgBr/Al-SBA-15 samples. Remarkably, the 40–60%Ag@AgBr/Al-SBA-15 samples had a significantly smaller specific surface area, pore volume, and pore diameter than the Al-SBA-15 support. The reason for this decrease could be the coverage of Ag@AgBr on the porous system that led to the decline in the specific surface area as well as the related parameters [22].

Fig. 4 (a) and (b) shows the SEM images of the Al-SBA-15 support and the 30%Ag@AgBr/Al-SBA-15 nanocomposite with averages sizes of 0.1–0.5 μm in diameter and a hexagonal and rod-like porous structure with a diameter of 0.1–0.5 μm, which was in good accordance with Al-SBA-15.

The TEM images shown in Fig. 4(a_1) and (b_1) also confirmed the presence of a 2D hexagonal array with well-ordered parallel straight mesochannels of the samples before and after loading the Ag@AgBr onto the Al-SBA-15 support, which agreed with the XRD and SEM results.

The optical properties of the 10–60%Ag@AgBr/Al-SBA-15 samples were investigated on the basis of UV–Vis absorption. As shown in Fig. 5A, a visible absorption band of around 300–800 nm was observed for all of the samples and assigned to the mixed peaks of the Ag@AgBr absorption.

Previous studies [41] have reported that AgBr, especially decorated with Ag nanoparticles, absorb light at the wavelength of approximately 510 nm, and therefore, the bandgap energy of the material can be deduced to be approximately 2.4 eV. However, with the Ag@AgBr/Al-SBA-15 samples synthesized by a chemical vapor deposition method, the absorption capacity in the visible-light region of the Ag@AgBr/Al-SBA-15 samples gradually shifted to longer wavelengths along with a considerably stronger absorption ability. This could be attributed to the synergistic effect of Ag and AgBr with different contents and the Al-SBA-15 support in the composites. Among the considered catalysts, the 30%Ag@AgBr/Al-MCM-41 sample had the highest light absorption ability. Subsequently, these spectra were converted into Kubelka-Munk functions, and the bandgap energy of the photocatalyst was obtained using Eq. (1).

$$\alpha h\nu = (Ah\nu - E_g)^{n/2} \quad (1)$$

where α, ν, E_g, and A are the absorption coefficient, light frequency, bandgap, and constant, respectively. In addition, n depends on the characteristics of the transition in a semiconductor, including direct transition ($n = 1$) or indirect transition ($n = 4$). Previous reports have indicated that Ag@AgBr is an indirect bandgap material. The bandgap energy can be estimated from a plot of

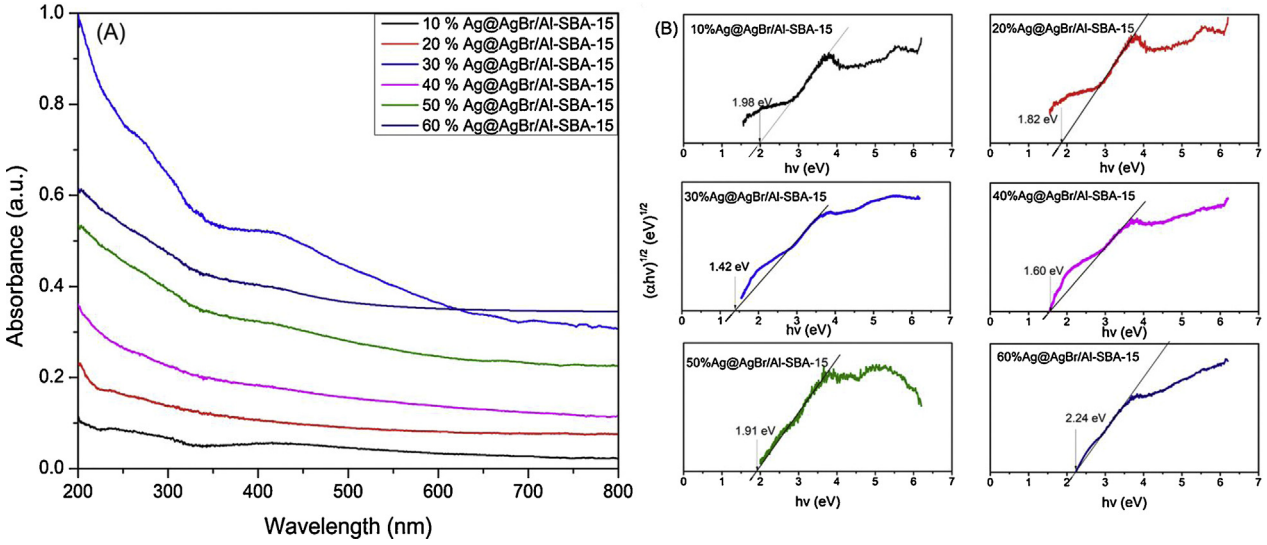

Fig. 5. (A) UV–Vis diffused reflectance spectra and (B) bandgap energies (E_g) of 10–60%Ag@AgBr/Al-MCM-41 photocatalysts.

Table 2
Optical properties of 10–60%Ag@AgBr/Al-SBA-15 samples.

Samples	Absorption edge (nm)	Bandgap energy (eV)
10%Ag@AgBr/Al-SBA-15	626.30	1.98
20%Ag@AgBr/Al-SBA-15	681.32	1.82
30%Ag@AgBr/Al-SBA-16	873.24	1.42
40%Ag@AgBr/Al-SBA-17	775.00	1.60
50%Ag@AgBr/Al-SBA-18	649.21	1.91
60%Ag@AgBr/Al-SBA-19	553.57	2.24

$(\alpha vh)^{1/2}$ versus the photon energy (hv) (Fig. 5B). The calculated results for the samples are presented in Table 2.

The 30%Ag@AgBr/Al-SBA-15 sample had the lowest bandgap energy, while the 60% Ag@AgBr/Al-SBA-15 sample had the highest. Thus, the bandgap energy of the obtained materials in the range of 1.42–2.24 eV was suitable for excitation in the sunlight area that could be promising for sulfur removal applications.

Photoluminescence (PL) was also employed to estimate the transfer and separation efficiency of photogenerated electron–hole pairs in the composite photocatalysts. As shown in Fig. 6, the major emission wavelength of the 10–60%Ag@AgBr/Al-SBA-15 samples were located at 460 nm. It can be seen that the emission intensity of the 30%Ag@AgBr/Al-SBA-15 catalyst had the weakest intensity. Theoretically, smaller PL intensity means lower recombination process of photogenerated electrons and holes, resulting in higher photocatalytic activity [42].

The surface chemical composition and chemical states of 30% Ag–AgBr/Al-SBA-15 nanocomposite were analyzed by XPS. Fig. 7 represents the wide XPS spectrum of 30%Ag–AgBr/Al-SBA-15, which shows the coexistence of Al 2p (at 30.5 eV), Br 3d (at 70.5 eV), Si 2p (at 104 eV). The high-resolution XPS spectra of Ag 3d demonstrates the appearance of both Ag $3d_{5/2}$ (at 367.65 and 368.35 eV) and Ag $3d_{3/2}$ (at 373.65 and 374.35 eV) in the sample. The peaks at 367.65 and 373.65 eV were attributed to Ag^{+}, while the peaks at 368.35 and 374.35 eV belong to Ag^{0} [43–45]. These results

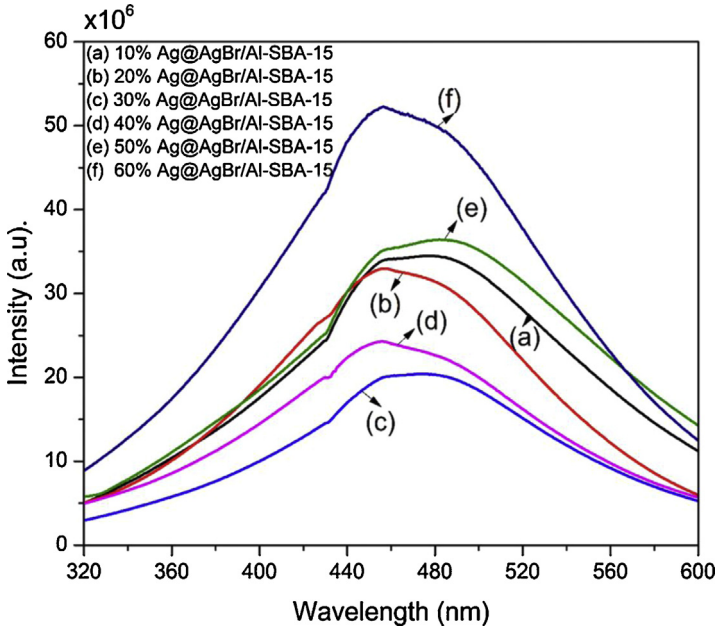

Fig. 6. Room temperature photoluminescence (PL) spectra of 10–60%Ag@AgBr/Al-SBA-15 samples.

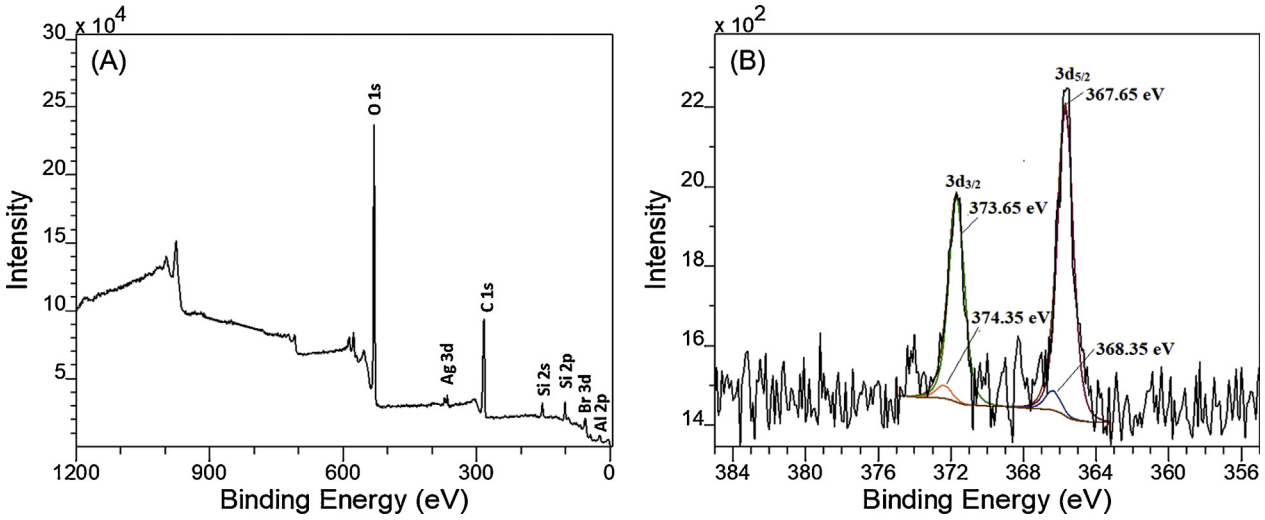

Fig. 7. XPS spectra of 30%Ag–AgBr/Al-SBA-15. (A) All elements and (B) Ag 3d.

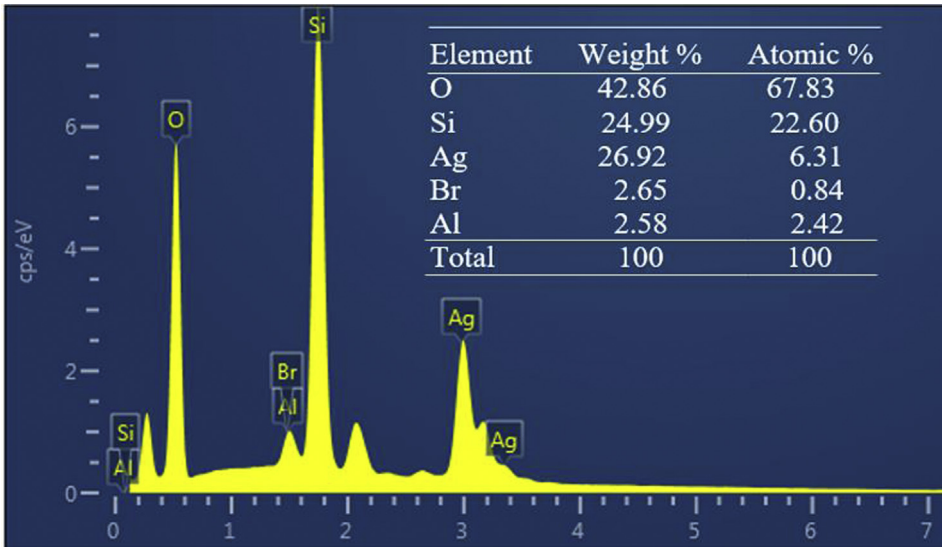

Fig. 8. Result of EDX analysis of 30%Ag@AgBr/Al-SBA-15 catalyst.

confirm the existence of Ag species and the interaction between Ag^0 and AgBr. In order to further explore the distribution and coexistence of elements present, the EDX of the 30%Ag@AgBr/Al-SBA-15 sample was carried out. As shown in Fig. 8, Si, Al, O, Ag and Br species were all detected in Ag@AgBr/Al-SBA-15 composite sample.

Photocatalytic activity of Ag@AgBr/Al-SBA-15 for the degradation of DBT

Photodegradation of DBT under sunlight irradiation

The photocatalytic activity of the 10–60%Ag@AgBr/Al-SBA-15 samples was investigated for DBT photodegradation under sunlight irradiation at 50 °C and 70 °C, with 50 mL of DBT (500 ppm of DBT concentration in *n*-octane), 1.0 mL of H_2O_2, and 50 mg of the photocatalyst. The photodegradation processes occurred after the adsorption of DBT on the catalyst had reached an equilibrium in the dark. The results presented in Fig. 9 revealed that during the 60 min dark period, samples showed an obvious adsorptive capacity for DBT, which was attributed to the adsorption of electron pairs of the sulfur atoms of DBT on the vacancies of silver, accordingly, to generate σ-coordinate bonds [46,47]. Furthermore, the 10–40%Ag@AgBr/Al-SBA-15 catalysts exhibited a better adsorptive capacity for DBT than 50–60% Ag@AgBr of these catalysts, which was attributed to the fact that the large BET specific surface area improved the dispersity of the active sites of Ag@AgBr on the support surface.

After sunlight irradiation for 360 min, the results indicated that increasing the Ag@AgBr content from 10% to 30% increased the desulfurization rate from 79.35% to 98.5% at 70 °C. However, when the Ag@AgBr content was increased from 40% to 60%, the efficiency of the DBT removal process decreased to 75.22% at 70 °C. This was also observed for the photocatalysts when the reaction was performed at 50 °C. The results showed that when the Ag@AgBr content was increased from 10% to 30%, the efficiency of the desulfurization increased from 50.86% to 69.72% after 360 min, and when the Ag@AgBr content was increased to 40–60%, the efficiency of the desulfurization decreased to 45.41%. Thus, no increase in the photocatalytic oxidative desulfurization efficiency at a high content of 40–60% Ag@AgBr could be attributed to the

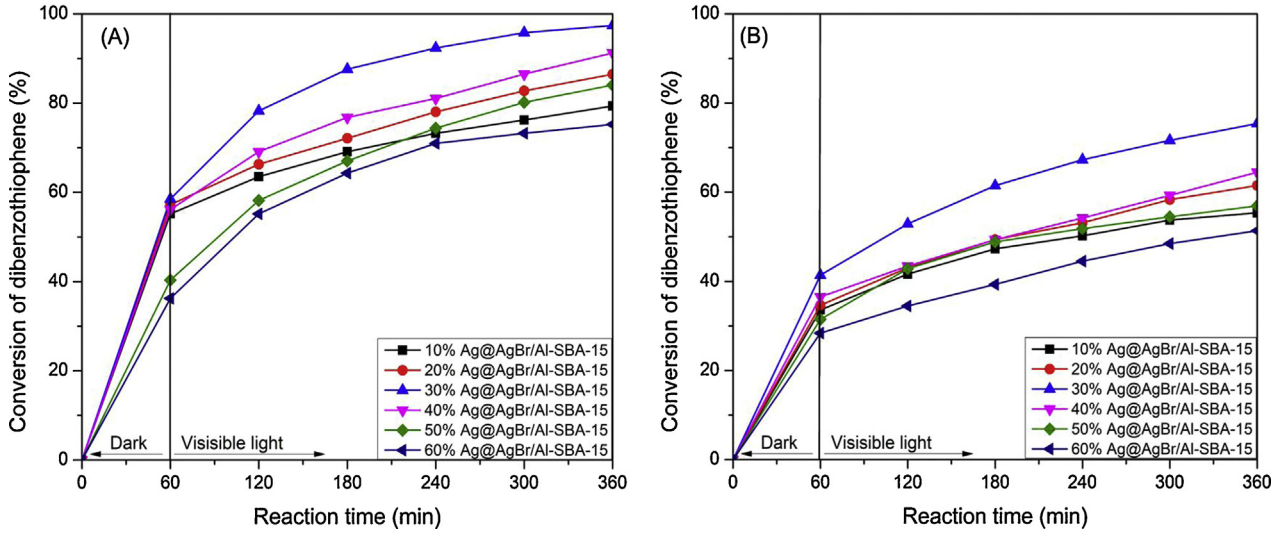

Fig. 9. Photodegradation of DBT with different photocatalyst contents under sunlight irradiation at reaction temperatures of (A) 70 °C and (B) 50 °C. (Reaction conditions: $V_{modeloil}$ = 50 mL, $m_{catalyst}$ = 50 mg, $V_{H_2O_2}$ = 1.0 mL).

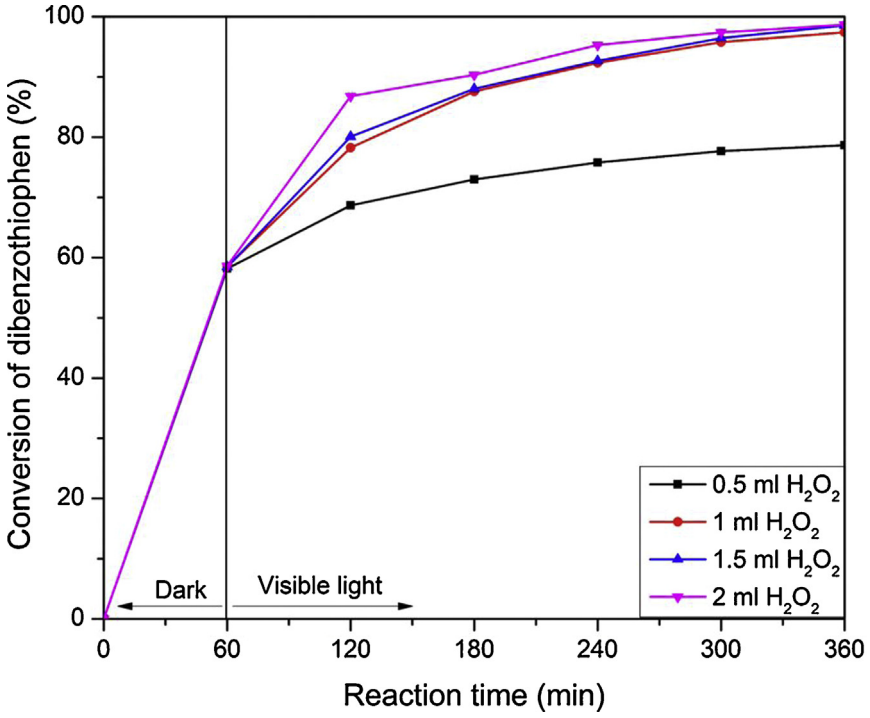

Fig. 10. Photodegradation of DBT by 30%Ag@AgBr/Al-SBA-15 catalyst at different H_2O_2 oxidant amounts under sunlight irradiation. (Reaction conditions: $V_{model\ oil}$ = 50 mL, $m_{catalyst}$ = 50 mg, reaction temperature = 70 °C).

accumulation of active sites on the surface that hindered the sulfide adsorption and oxidation. The 30%Ag–AgBr/Al-SBA-15 catalyst exhibited the highest activity with a DBT conversion that reached 98.5% at 70 °C after 360 min because it had the lowest bandgap energy (E_g = 1.42 eV). This is in good agreement with the PL results (Fig. 6) which demonstrated that the emission intensity of the 30%Ag@AgBr/Al-SBA-15 catalyst has the weakest intensity.

According to Jiang et al. [48], hole and •OH serve as the main active species involved in the photodegradation of organic compounds in AgBr@Ag, and electrons in the lowest unoccupied orbital of Ag^0 could be excited by the strong surface plasmon resonance (SPR) effect:

$$Ag + h\upsilon \rightarrow \overline{e} + Ag^{+}. \quad (2)$$

Therefore, photogenerated electrons from Ag^+ could easily be transferred to the conduction band (CB) of AgBr and to the surface of the Al-SBA-15 support, where the electrons were trapped by the surface-absorbed O_2 molecules to form $O_2^{-\bullet}$, as described in Eq. (3):

$$(3)O_2 + \overline{e} \rightarrow O_2^{-\bullet}$$Moreover, AgBr could respond to sunlight with a narrow bandgap to generate the electron–hole pairs:

$$AgBr + h\upsilon \rightarrow AgBr(\overline{e} + h^{+}). \quad (4)$$

The photogenerated holes with a strong oxidizing ability could react with H_2O molecules to generate •OH radical:

$$h^{+} + H_2O \rightarrow {}^{\bullet}OH \quad (5)$$

or directly degrade DBT to products. This could be justified by the reduction of the BET surface area and the pore volume of the samples of 40–60%Ag@AgBr/Al- SBA-15 as compared to those in the case of the other samples.

The results showed that with an increase in Ag@AgBr content from 10% to 30%, the efficiency of desulfurization increased from 50.86% to 69.72% at 50 °C after 360 min. However, when the Ag@AgBr content was increased to 40–60%, the efficiency of desulfurization decreased to 45.41% at 50 °C. This could be explained by the reduced surface area of the samples as compared to that of the samples with 10–30% of the Ag@AgBr loading. The 30%Ag–AgBr/Al-SBA-15 catalyst exhibited the highest photocatalytic activity because it had the lowest bandgap energy and its surface area was equal to that of the 10–20%Ag–AgBr/Al-SBA-15 samples, which had the highest value. The maximum DBT conversion obtained in this case was 98.66% at 70 °C.

Moreover, the presence of the oxidizing agent had a decisive influence on the process. Fig. 10 displays the DBT conversion on the 30%Ag@AgBr/Al-SBA-15 catalyst after 360 min with the addition of H_2O_2. The conversion reached only 78.67% with 0.5 mL of H_2O_2 added. It is well-known that H_2O_2 is a strong oxidizing agent and produces hydroxyl radicals when exposed to light. However, using an excessive amount of H_2O_2 will poison the Ag@AgBr/Al-SBA-15 catalyst surface, leading to the side effects of the photocatalytic reaction. This resulted in the generation of optimum hydroxyl radicals for the oxidation of DBT obtained by the addition of approximately 0.5 mL of H_2O_2. When low concentrations of H_2O_2 (<0.5 mL) were used, the reaction between the hydroxyl radicals and H_2O_2 occurred; therefore, the •OH radicals needed to facilitate oxidation reaction became rare in this case. Correspondingly, the yield of sulfur removal was small when a small quantity of the oxidizing agent was used. Meanwhile, with an increase in the amount of H_2O_2 from 1.0 to 2.0 mL, the conversion of DBT remained almost unchanged and reached the highest sulfur removal efficiency of 98.66% after 360 min, which might be attributed to an unwanted coverage of active sites by a higher number of oxygen free radicals from the oxidizing agent of H_2O_2.

The effect of temperature on the photodegradation performance was greatly reflected in the dark adsorption. Therefore, the photocatalytic activity of 30%Ag@AgBr/Al-SBA-15 photocatalyst was evaluated for degradation of DBT in the dark, and the obtained results are shown in Fig. 11. Reference experiments showed that no photocatalytic reaction occurs in the presence of the photocatalyst without sunlight irradiation. Only, 35.43%, 44.21%, 53.43% and 58.98% of DBT were adsorbed at temperatures of 40 °C, 50 °C, 60 °C,

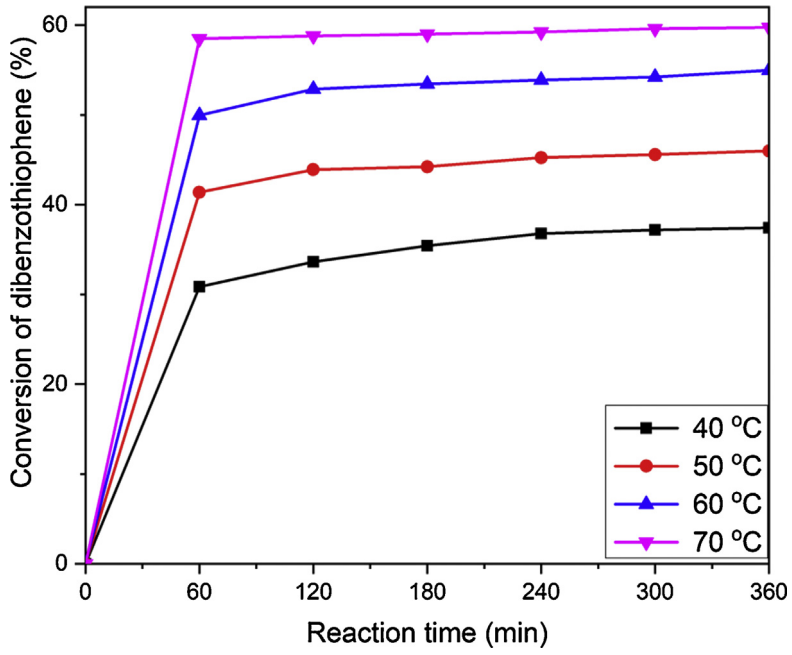

Fig. 11. Effect of reaction temperature on photodegradation of DBT in the dark (Reaction conditions: $V_{\text{model oil}} = 50$ mL, $m_{\text{catalyst}} = 50$ mg, $V_{H_2O_2} = 1.0$ mL).

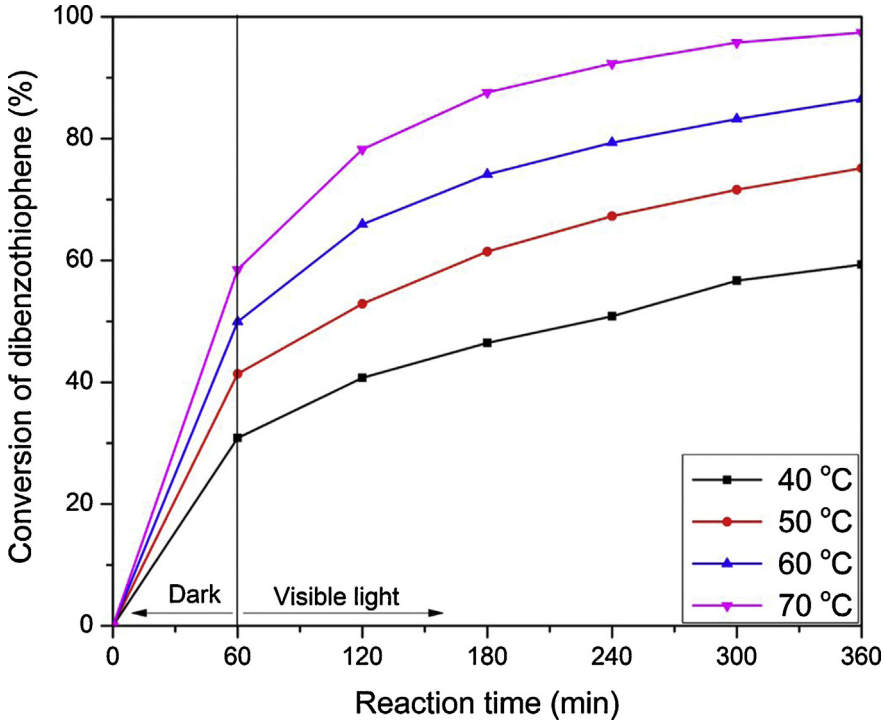

Fig. 12. Photodegradation of DBT by 30%Ag@AgBr/Al-SBA-15 catalyst at different temperatures under sunlight irradiation. (Reaction conditions: $V_{\text{modeloil}} = 50$ mL, $m_{\text{catalyst}} = 50$ mg, $V_{H_2O_2} = 1.0$ mL).

and 70 °C, respectively for 3 h, and adsorption of DBT remained unchanged for 6 h. This indicates that the activity of the composite photocatalyst was due to the production of •OH radicals under sunlight irradiation causing the DBT degradation.

As mentioned above, temperature was an important factor in the oxidation desulfurization in this study. Here, the reaction temperature varied between 40 °C and 70 °C, and the result is presented in Fig. 12. We observed that the conversion of DBT increased with an increase in the reaction temperature. The conversion of DBT oxidation at 70 °C was approximately two times higher than that at 40 °C for all the investigated reaction times and reached 98.5% after 360 min. This was because of the difference in the number of hydroxyl radicals at different temperatures. At 70 °C, the generation rate of hydroxyl radicals (•OH) was higher than that at 40 °C, allowing for higher DBT reduction through oxidation on the catalyst surface. In addition, the DBT oxidation was limited by kinetics because of the diffusion restriction at temperatures below 50 °C.

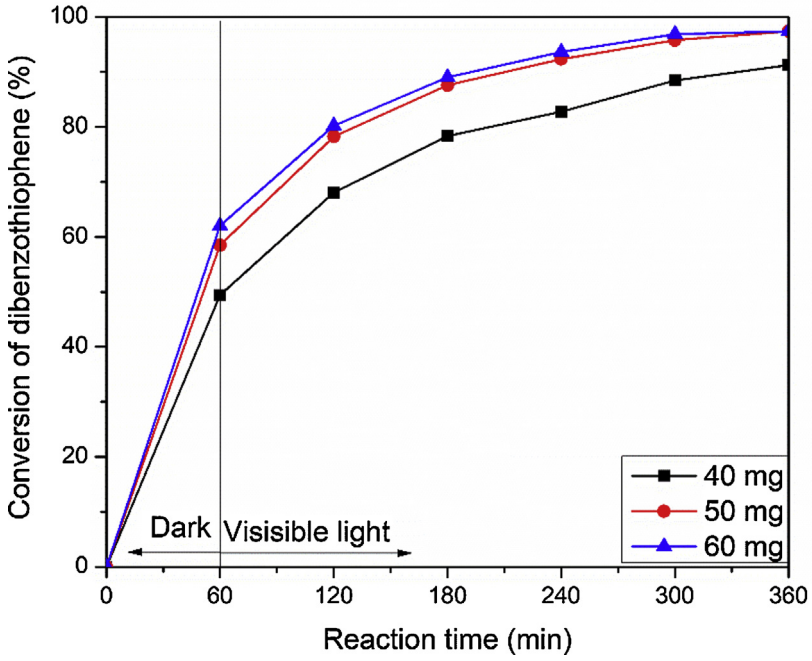

Fig. 13. Photodegradation of DBT by 30%Ag@AgBr/Al-SBA-15 catalyst at different amount of catalyst under sunlight irradiation. (Reaction conditions: $V_{\text{model oil}} = 50$ mL, $V_{H_2O_2} = 1.0$ mL, reaction temperature of 70 °C).

Fig. 13 shows the effect of catalyst dosage on the DBT degradation under sunlight irradiation. Increasing the amount of 30%Ag@AgBr/Al-SBA-15 catalyst from 40 to 50 mg leads to an increase in the photodegradation of DBT. In this case, the increased catalytic active sites could enhance the generation and transfer of photogenerated charge carriers. However, when increasing catalyst dosage further to 60 mg, a very little change was observed on the conversion of DBT, demonstrating that most DBT in 50 mL was photodegraded using ~50 mg catalyst at 70 °C.

Kinetics of photocatalytic degradation

From the abovementioned experiments, all the optimal reaction conditions were used in the system, i.e., 1.0 mL of H_2O_2, 50 mL of DBT (500 ppm DBT in *n*-octane), 50 mg of 30%Ag@AgBr/Al-SBA-15, and operating temperatures of 40 °C, 50 °C, 60 °C, and 70 °C. The photocatalytic degradation of DBT as a function of irradiation time in the presence of 30%Ag@AgBr/Al-SBA-15 could be described by the pseudo first-order reaction, as shown in Eq. (6):

$$-\ln\left(\frac{C_t}{C_0}\right) = k_p t \tag{6}$$

where C_t and C_0 are the concentrations at time t and time zero, respectively, k_p is the first-order reaction rate constant (h^{-1}), and t is the irradiation time (h). The data shown in Fig. 14 could be satisfactorily analyzed by the first-order kinetic Eq. (6) to obtain the rate constant.

According to Fig. 14A, the first-order kinetic equation of the desulfurization reaction of 30%Ag@AgBr/Al-SBA-15 was determined at different temperatures. That is, $y = 0.00917x + 0.05842$

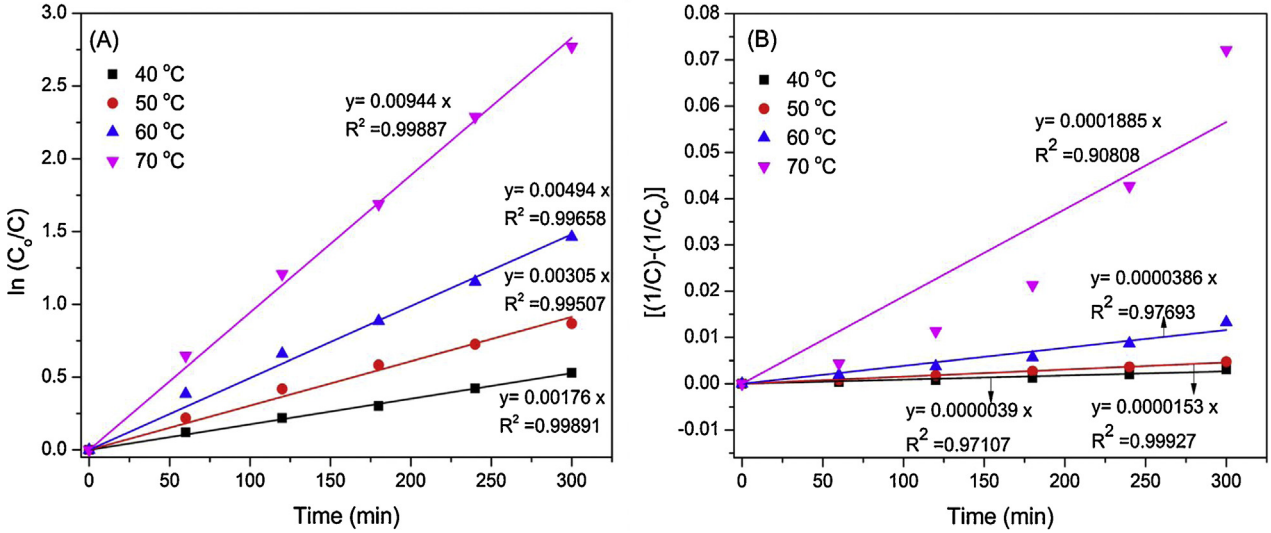

Fig. 14. Plot of (A) pseudo first-order and (B) pseudo second-order kinetic models for the degradation of DBT by photocatalytic oxidative desulfurization at different temperatures.

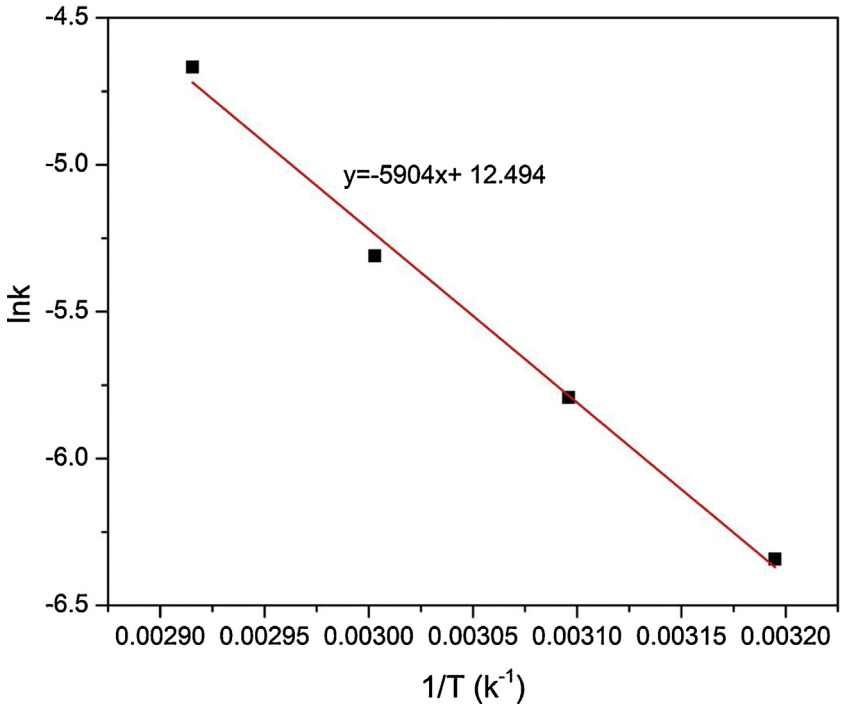

Fig. 15. Arrhenius plot for the photocatalytic degradation of DBT.

with the value of correlation coefficient $R^2 = 0.99762$, $y = 0.00469x + 0.0546$ with the value of correlation coefficient $R^2 = 0.99272$, $y = 0.00287x + 0.03889$ with the value of correlation coefficient $R^2 = 0.98878$, and $y = 0.00173x + 0.0577$ with a correlation coefficient $R^2 = 0.99975$ at temperatures of 70 °C, 60 °C, 50 °C, and 40 °C, respectively. All the linear graphs agreed with the first-order reaction ($R^2 > 0.98$). The kinetic rate constants (k_p) of 70 °C, 60 °C, 50 °C, and 40 °C were measured at 0.5502, 0.2814, 0.1722, and 0.1038 h^{-1}, respectively. The half-life of the experiment was calculated by substituting C_t with $C_0/2$. The obtained results are shown in Eq. (7).

$$t_{1/2} = \frac{0.693}{k_p} \tag{7}$$

where $t_{1/2}$ is the half-life (h).

According to the kinetics study, the half-life ($t_{1/2}$) of the DBT degradation reactions were determined to be 1.26, 2.46, 4.03, and 6.68 h at the reaction temperatures of 70 °C, 60 °C, 50 °C, and 40 °C,

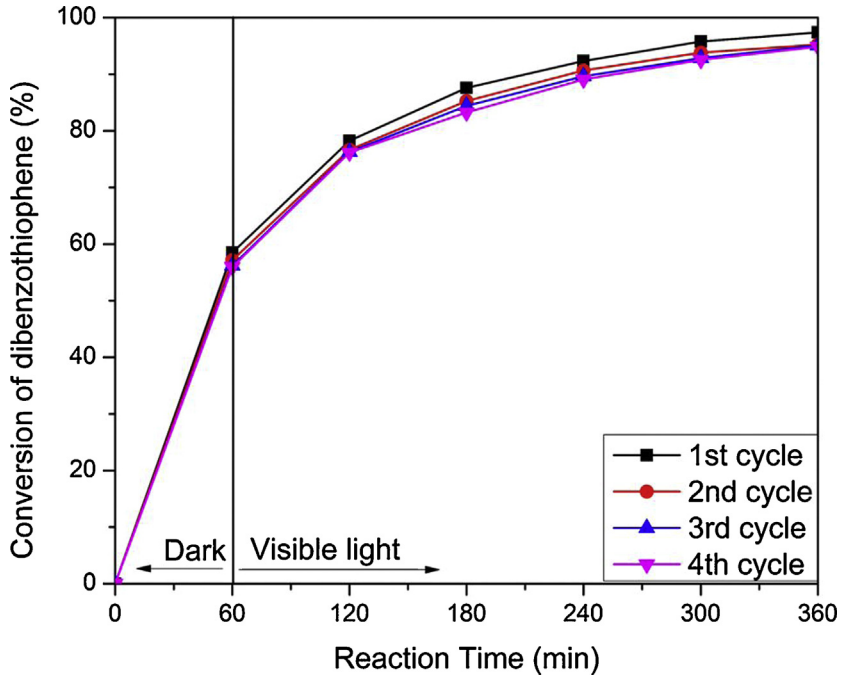

Fig. 16. Photocatalytic degradation of DBT in successive cycles by 30%Ag@AgBr/Al-SBA-15. (Reaction conditions: $V_{modeloil} = 50$ mL, $m_{catalyst} = 50$ mg, $V_{H_2O_2} = 1.0$ mL, at a reaction temperature of 70 °C).

respectively. These results indicated that as the relatively fast degradation rate of DBT increased, the reaction temperature increased (70 °C), which agreed with the increases in the reaction temperature and the reaction rate according to the Arrhenius equation (5) [49,50] and resulted in a higher conversion of DBT.

Thus, the oxidative photocatalytic desulfurization for DBT in the *n*-octane solvent using 30%Ag@AgBr/Al-SBA-15 was the pseudo first-order reaction.

In contrast, if the reaction followed the second-order kinetics, the kinetic equation could be expressed as follows:

$$\frac{1}{[C]^{n-1}} = \frac{1}{[C_0]^{n-1}} + (n-1)kt \tag{8}$$

where C_t and C_0 are the concentrations at time t and time zero, respectively, k is the second-order reaction rate constant, t is the irradiation time (h), and n is the reaction order ($n = 2$ for the second-order equation). Plots were built to identify the relationship between $[(1/C) - (1/C_0)]$ versus the irradiation time at different temperatures, as shown in Fig. 14B.

As calculated, the second-order reaction did not seem to be suitable for sulfur removal. Indeed, the kinetic data collected at 70 °C yielded a considerably low correlation coefficient with the value of $R^2 = 0.86$. In addition, the values obtained at 40 °C, 50 °C and 60 °C did not converge, which showed an important fluctuation. These R^2 values were considerably lower in the pseudo second-order reaction than in the pseudo first-order kinetic reaction model ($R^2 > 0.98$), and the confidence value was insignificant for the former; hence, the pseudo second-order reaction model was not considered for the photocatalytic degradation of DBT under sunlight irradiation.

The dependence of the rate constant k on the reaction temperature was expressed as an Arrhenius equation:

$$k = Ae^{-\frac{E_a}{RT}} \tag{9}$$

Accordingly,

$$\ln\ k = -\frac{E_a}{R}\left(\frac{1}{T}\right) + \ln\ A \tag{10}$$

where E_a is the apparent activation energy, A is the pre-exponential factor, R is the gas, and T is the reaction temperature (K). The Arrhenius plot considering the first-order reaction is shown in Fig. 15. The apparent activation energy (E_a) was calculated from the slope and the intercepts of the Arrhenius plot with a value of 48.93 kJ/mol. This value was similar to previously reported results; where the activation energy was 52.83 kJ/mol for DBT oxidation in H_2O_2/acetic acid using polyoxometalates as catalysts [51]. Mohammad et al. [52] reported that the E_a value for the oxidative desulfurization of DBT was 57.54 kJ/mol by using a new sandwich-

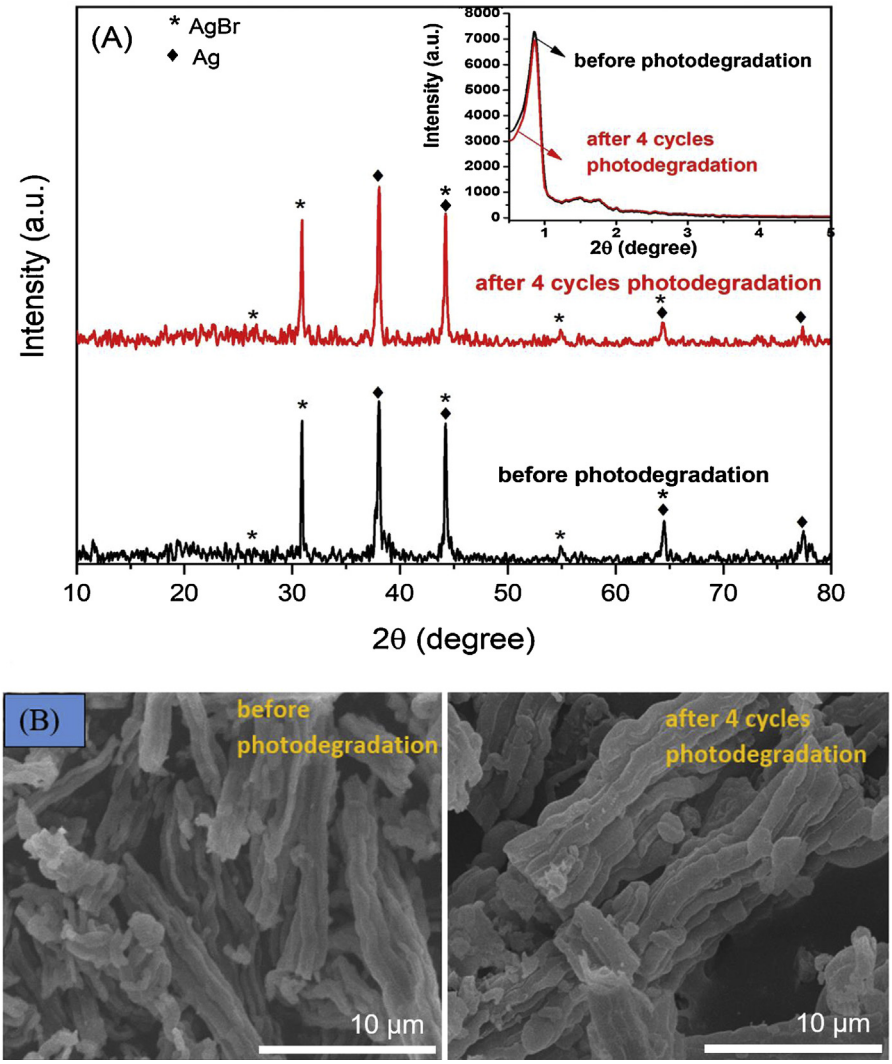

Fig. 17. (A) XRD patterns and (B) SEM images of 30%Ag@AgBr/Al-SBA-15 before and after four cycles of DBT photodegradation.

type polyoxometalate/nanoceramic nanocomposite. Lorena et al. [53] applied the pseudo first-order rate constants for the oxidation of DBT at different temperatures and obtained an E_a value of 43.4 kJ/mol.

Stability of the photocatalyst

To evaluate the reusability, the circulating runs in the photodegradation of DBT over the 30%Ag@AgBr/Al-SBA-15 catalyst were reused four times for the photocatalysis (Fig. 16). After the subsequent runs under sunlight, the DBT photocatalytic degradation effectiveness slightly decreased from 97.40% to 94.88%, indicating that the photocatalytic activity of 30%Ag@AgBr/Al-SBA-15 remained steady. The XRD patterns (Fig. 17A) and the SEM images (Fig. 17B) confirm that no obvious crystal structure and morphology changes are observed in the 30%Ag@AgBr/Al-SBA-15 catalyst after the fourth photodegradation cycle.

Conclusions

The photocatalytic oxidation desulfurization of a model fuel by Ag@AgBr/Al-SBA-15 was investigated under sunlight irradiation. The optimal content of 30%Ag@AgBr loaded on the Al-SBA-15 exhibited an outstanding photocatalytic activity for the degradation of DBT, which could be preceded via the strong adsorption performance of the Al-SBA-15 support and the direct reaction of DBT with the photogenerated $\bar{e}$–h^+ pairs under sunlight irradiation. In these investigations, the sulfur removal of 98.66% was achieved for DBT after 360 min at an operating temperature of 70 °C, 1.0 mL of H_2O_2 (30 v/v%), and 50 mg of catalyst. The photocatalyst possessed good stability and reusability under sunlight irradiation for four successive cycles.

Declaration of Competing Interest

The authors report no declarations of interest.

Acknowledgment

This work was financially supported by the National Foundation for Science and Technology Development of Vietnam (Grant No. 105.99-2018.301).

Appendix A. Supplementary data

Supplementary data associated with this article can be found, in the online version, at https://doi.org/10.1016/j.jiec.2020.07.037.

References

[1] M.A.A. Amparan, L.C. Caero, Catal. Today 282 (2017) 133.
[2] C.S. Song, Today 86 (2003) 211.
[3] J. Carbajo, A. Bahamonde, M. Faraldos, Mol. Catal. 434 (2017) 167.
[4] F.C. Javier, B.M. Ángel, C.A. Diego, Materials 11 (2018) 1149.
[5] X. Chen, S. Shen, L. Guo, S.S. Mao, Chem. Rev. 110 (2010) 6503.
[6] L.G. Devi, R. Kavitha, Appl. Catal. B Environ. 140–141 (2013) 559.
[7] L. Zhu, J. Ji, J. Liu, S. Mine, M. Matsuoka, J. Zhang, M. Xing, Angew. Chem. Int. Ed. (2020), doi:http://dx.doi.org/10.1002/anie.202006059.
[8] J. Ji, R.M. Aleisa, H. Duan, J. Zhang, Y. Yin, M. Xing, Science 23 (2020) 100861.
[9] Q. Yi, J. Ji, B. Shen, C. Dong, J. Liu, J. Zhang, M. Xing, Environ. Sci. Technol. 53 (2019) 9725.
[10] P. Selvakannan, K. Mantri, J. Tardio, S.K. Bhargava, J. Colloid Interface Sci. 394 (2013) 475.
[11] K. Mori, P. Verma, R. Hayashi, Chem. Eur. J. 21 (2015) 11885.
[12] P.C. Nagajyothi, M. Pandurangan, S.V.P. Vattikuti, C.O. Tettey, T.V.M. Sreekanth, J. Shim, Sep. Purif. Technol. 188 (2017) 228.
[13] V. Vaiano, M. Matarangolo, J.J. Murcia, H. Rojas, J.A. Navío, M.C. Hidalgo, Appl. Catal. B-Environ. 225 (2018) 197.
[14] M. Zarrab, M.H. Entezari, J. Colloid Interface Sci. 457 (2015) 353.
[15] M. Pirhashemia, A. Habibi-Yangjeha, S.R. Pouranb, J. Ind. Eng. Chem. 62 (2018) 1–25.
[16] M. Shekofteh-Gohari, A. Habibi-Yangjeh, M. Abitorabi, A. Rouhi, Crit. Rev. Environ. Sci. Technol. 48 (2018) 10–12.
[17] H. Tang, S.-F. Chang, G.-G. Tang, W. Liang, Appl. Surf. Sci. 391 (2017) 440.
[18] M. Mousavi, A. Habibi-Yangjeh, S.R. Pouran, J. Mater. Sci. Mater. Electron 29 (2018) 1719–1747.
[19] A. Akhundi, A. Badiei, G.M. Ziarani, A. Habibi-Yangjehc, M.J. Muñoz-Batistad, R. Luque, Mol. Catal. 488 (2020) 110902.
[20] A. Akhundi, A. Habibi-Yangjeh, M. Abitorabi, S.R. Pouran, Catal. Rev. 61 (2019) 595–628.
[21] Y. Xu, H. Xu, J. Yan, H. Li, L. Huang, J. Xia, S. Yin, H. Shu, Physicochem. Eng. Asp. 436 (2013) 474.
[22] X.N. Pham, B.M. Nguyen, T.T. Hoa, H.V. Doan, Adv. Powder Technol. 29 (2018) 1827.
[23] M.-M. Liu, L.-A. Hou, B.-D. Xi, Q. Li, X.-J. Hu, S.-L. Yu, Chem. Eng. J. 302 (2016) 475.
[24] L.-Q. Ye, J.-Y. Liu, C.-Q. Gong, L.-H. Tian, T.-Y. Peng, L. Zan, ACS Catal. 2 (2012) 1677.
[25] J.G. McEvoy, Z. Zhang, J. Photochem. Photobiol. A 321 (2016) 161.
[26] M. Zhu, P. Chen, M. Liu, Langmuir 28 (2012) 3385.
[27] M.A. Asi, L. Zhu, C. He, V.K. Sharma, D. Shu, S. Li, J. Yang, Y. Xiong, Catal. Today 216 (2013) 268.
[28] L. Hu, H. Yuan, L. Zou, F. Chen, X. Hu, Appl. Surf. Sci. 355 (2015) 706.
[29] V.K. Tomer, P.V. Adhyapak, S. Duhan, I.S. Mulla, Microporous Mesoporous Mater. 197 (2014) 140.
[30] X.N. Pham, D.L. Tran, T.D. Pham, Q.M. Nguyen, V.T.T. Thi, H.V. Doan, Adv. Powder Technol. 29 (2018) 58.
[31] X.N. Pham, H.V. Doan, Chem. Eng. Commun. 206 (2019) 1139.
[32] T. Yanagisawa, T. Shimizu, K. Kuroda, C. Kato, B. Chem. Soc. Jpn. 63 (1990) 988.
[33] F. Kang, Q. Wang, S. Xiang, Mater. Lett. 59 (2005) 1426.
[34] P. Kumar, N. Mal, Y. Oumi, K. Yamana, T. Sano, J. Mater. Chem. 11 (2001) 3285.
[35] H. Yang, Y. Deng, C. Du, S. Jin, Appl. Clay Sci. 47 (2010) 351.
[36] X.N. Pham, T.D. Pham, B.M. Nguyen, H.T. Tran, D.T. Pham, J. Chem. (2018) 9 ID 8418605.
[37] C. Zhou, T. Sun, Q. Gao, A. Alshameri, P. Zhu, H. Wang, X. Qiu, Y. Ma, C. Yan, J. Taiwan Inst. Chem. E. 45 (2014) 1073.
[38] S.M.L. Santos, K.A.B. Nogueira, M.S. Gama, J.D.F. Lima, I.J.S. Júnior, D.C.S. Azeved, Microporous Mesoporous Mater. 180 (2013) 284.
[39] H.-A. Rafael, N. Rufino, L.P.-L. Carmen, L.-R. Javier, A.-N. Gabriel, P. Barbara, M. R.-M. Eric, Materials 6 (2013) 4139.
[40] D.J. Kim, M. Pal, W.S. Seo, Microporous Mesoporous Mater. 180 (2013) 32.
[41] Y. Guan, S. Wang, X. Wang, C. Sun, Y. Huang, C. Liu, H. Zhao, Appl. Catal. B Environ. 209 (2017) 329.
[42] X. Xiaoa, L. Gea, C. Han, Y. Li, Z. Zhao, Y. Xin, S. Fang, L. Wu, P. Qiu, Appl. Catal. B Environ. 163 (2015) 564–572.
[43] C. An, S. Peng, Y. Sun, Adv. Mater. 22 (2010) 2570–2574.
[44] Y. Hou, F. Zuo, Q. Ma, C. Wang, L.D. Bartels, P.Y. Feng, J. Phys. Chem. C 116 (2012) 20132–20139.
[45] L.H. Dong, S.S. Tang, J.Y. Zhu, P.Y. Zhan, L.F. Zhang, F.W. Tong, Mater. Lett. 91 (2013) 245–248.
[46] B. Saha, S. Kumar, S. Sengupta, Chem. Eng. Sci. 199 (2019) 332.
[47] X. Li, Y. Xua, C. Zhang, H. Wang, Y. Song, W. Zhang, C. Li, Fuel 226 (2018) 527.
[48] J. Jiang, H. Li, L.-Z. Zhang, Chem. Eur. J. 18 (2012) 6360.
[49] D. Xie, Q. He, Y. Su, T. Wang, R. Xu, B. Hu, Chinese J. Catal. 36 (2015) 1205.
[50] H. Li, W. Zhu, J. Lu, X. Jiang, L. Gong, G. Zhu, Y. Yan, React. Kinet. Catal. Lett. 96 (2009) 165.
[51] C. Komintarachat, W. Trakarnpruk, Ind. Eng. Chem. Res. 45 (2006) 1853.
[52] A.R. Mohammad, K. Sahar, Solid State Sci. 98 (2019) 106036.
[53] P.R. Lorena, A.V. Verónica, C.L. Brenda, V.P. María, L.M. María, A.A. Oscar, R.B. Andrea, Catal. Today 271 (2016) 102.